Spectrochimica Acta Part A 78 (2011) 1548–1552

Contents lists available at ScienceDirect

Spectrochimica Acta Part A: Molecular and Biomolecular Spectroscopy

journal homepage: www.elsevier.com/locate/saa

Effects of spin transitions degeneracy in pulsed EPR of the fullerene C_{70} triplet state produced by continuous light illumination

Mikhail N. Uvarov[a], Leonid V. Kulik[a,*], Tatiana I. Pichugina[a,b], Sergei A. Dzuba[a,b]

[a] Institute of Chemical Kinetics and Combustion, Institutskaya 3, 630090 Novosibirsk, Russia
[b] Novosibirsk State University, Pirogova 2, 630090 Novosibirsk, Russia

ARTICLE INFO

Article history:
Received 6 October 2010
Received in revised form
23 December 2010
Accepted 26 January 2011

Keywords:
Electron spin echo
Density matrix formalism
Triplet state
Spin polarization
Fullerene

ABSTRACT

X-band echo-detected electron paramagnetic resonance (ED EPR) spectra of triplet state of fullerene C_{70} generated by continuous light illumination were found to correspond below 30 K to a non-equilibrium electron spin polarization. Above 30 K spectra are characteristic of Boltzmann equilibrium. Spectra were simulated fairly well with zero-field splitting parameters $D = 153$ MHz and E and distributed within the range of 6–42 MHz. The origin of E distribution is attributed to the Jahn–Teller effect, which in glassy matrix is expected to depend on the local surrounding of a fullerene molecule (a so-called E-strain). In the center of ED EPR spectra a narrow hole was observed. With increase of the microwave pulse turning angle this hole transforms into a single narrow absorptive line. Numerical simulations by density matrix formalism confirm that central hole originates from a simultaneous excitation of both allowed electron spin transitions of the triplet ($T_0 \leftrightarrow T_+$ and $T_0 \leftrightarrow T_-$), because of their degeneracy at this spectral position. Also explanations are given why this hole has not been observed in the previously reported experiments on continuous wave EPR and on ED EPR under laser pulse excitation.

1. Introduction

The unique photophysical properties of fullerenes and their derivatives allow to suggest different practical applications of these materials [1,2]. The triplet fullerenes can also be used as spin probes to provide information about properties of glass matrices [3,4].

For the triplet state of C_{70}, $^3C_{70}$, the zero-field splitting (ZFS) parameters, D and E, were found at liquid helium temperature to be 155 MHz (5.5 mT) and 21 MHz (0.75 mT), respectively [5]. The lifetime of the first excited triplet state in toluene was found to be 51 ms at 77 K [5], and 11.8 ms at room temperature [6]. The spin-density distribution among different carbon atoms in $^3C_{70}$ was determined [7]. The $^3C_{70}$ EPR lineshape and triplet spin relaxation mechanisms were discussed [4,5,8–11]. Anisotropy of spin-lattice relaxation in $^3C_{70}$ was observed [8,10]. Temperature dependence of EPR lineshape was simulated using model of $^3C_{70}$ molecular pseudorotations [9–11].

Previous EPR investigations of $^3C_{70}$ have been performed mostly with time-resolved EPR and electron spin echo (ESE) techniques, using photoexcitation by a laser pulse. In the present work we demonstrate that $^3C_{70}$ can be observed with ESE spectroscopy under continuous light illumination. The $^3C_{70}$ triplet state lifetime is long enough to allow the observation of echo signals of $^3C_{70}$ even in thermally equilibrium state, i.e., when Boltzmann distribution of populations within triplet spin sublevels takes place.

Note that in experiments in which $^3C_{70}$ is produced by laser pulse, ESE signal in thermal equilibrium is not observed because of the unfavorable ratio between the $^3C_{70}$ decay rate and the laser repetition rate. In contrast to ESE, in time-resolved EPR spectra in thermal equilibrium may be observed, under detection with a long delay after the laser flash.

We found in this work that X-band echo-detected (ED) EPR spectra of $^3C_{70}$ produced by continuous light illumination manifest new features in the central region of the spectra, which do not present in time-resolved EPR. These features cannot be simulated within a commonly used approach when two microwave (mw) transitions are treated independently (a two-level system approximation).

2. Theoretical background

Spin Hamiltonian of a molecule in a triplet state is a sum of the Zeeman Hamiltonian and the Hamiltonian of magnetic dipole–dipole interaction of two unpaired electron spins ($\boldsymbol{H}_\mathbf{D}$) [12]:

$$\boldsymbol{H}_\mathbf{0} = g\beta \boldsymbol{B}_\mathbf{0} \boldsymbol{S} + \boldsymbol{H}_\mathbf{D}, \quad (1)$$

where $\boldsymbol{B}_\mathbf{0}$ is the magnetic field, $\boldsymbol{S}$ is the spin operator ($S = 1$), β is the Bohr magneton, g is g-factor, which for $^3C_{70}$ may be assumed isotropic with good accuracy, $\boldsymbol{H}_\mathbf{D} = 1/2 S_i D_{ij} S_j$, where D_{ij} is the com-

* Corresponding author. Tel.: +7 383 333 22 97; fax: +7 383 330 73 50.
E-mail address: chemphy@kinetics.nsc.ru (L.V. Kulik).

1386-1425/$ – see front matter © 2011 Elsevier B.V. All rights reserved.
doi:10.1016/j.saa.2011.01.047

ponent of the zero-field splitting (ZFS) tensor. In the molecular framework (x, y, z)

$$\boldsymbol{H}_{\mathbf{D}} = D\left(S_z^2 - \frac{1}{3}\boldsymbol{S}^2\right) + E(S_x^2 - S_y^2),$$

where D and E are the ZFS parameters. In the molecular framework, $\boldsymbol{B_0} = B_0(\sin\theta\cos\varphi, \sin\theta\sin\varphi, \cos\theta)$, where θ and φ are respectively the polar and the azimuthal angles determining the orientation of the $\boldsymbol{B_0}$ vector. In the laboratory framework (X, Y, Z), where Z axis is parallel to the external magnetic field

$$\boldsymbol{H}_{\mathbf{D}} = \frac{1}{2}\left(\frac{D}{3}(3\cos^2\theta - 1) + E\sin^2\theta\cos 2\varphi\right)(3S_z^2 - \boldsymbol{S}^2).$$

For $^3C_{70}$ at X-band EPR the high-field approximation takes place, $g\beta B_0 \gg D$. Energies of the two allowed transitions between adjacent eigenstates of the Hamiltonian (Eq. (1)), $T_0 \leftrightarrow T_+$ and $T_0 \leftrightarrow T_-$, are [3]:

$$\begin{aligned}\hbar\omega_{0+} &= g\beta B_0 + \frac{D}{2}(3\cos^2\theta - 1) + \frac{3E}{2}\sin^2\theta\cos 2\varphi;\\ \hbar\omega_{0-} &= g\beta B_0 - \frac{D}{2}(3\cos^2\theta - 1) - \frac{3E}{2}\sin^2\theta\cos 2\varphi,\end{aligned} \quad (2)$$

respectively, where $\hbar$ is the Plank constant. As can be easily derived from Eq. (2), the degeneracy of the allowed triplet transitions for polyoriented triplets occurs, when $\hbar\omega_{0+} = \hbar\omega_{0-} = g\beta B_0$. This condition corresponds to the position in center of the EPR spectrum of the triplet.

In the rotating laboratory framework, the Hamiltonian of the triplet molecule is

$$\boldsymbol{H_0} = \hbar(\gamma B_0 - \omega)S_z - \frac{3}{2}\left(D\left(\frac{1}{3} - \cos^2\theta\right) - E\cos 2\varphi\sin^2\theta\right)S_z^2, \quad (3)$$

where ω is the microwave frequency (frequency of the framework rotation), $\gamma = g\beta$ is the gyromagnetic ratio.

During the microwave pulse, the Hamiltonian is

$$\boldsymbol{H_p} = \boldsymbol{H_0} + \hbar\omega_1 S_x, \quad (4)$$

where $\omega_1 = g\beta B_1/\hbar$.

For a system in thermodynamic equilibrium the density matrix is [13]

$$\boldsymbol{\rho_0} = \frac{1}{Sp\mathbf{1}}\left(\mathbf{1} - \frac{\boldsymbol{H_0}}{kT}\right),$$

where T is the temperature, $\mathbf{1}$ is the unity matrix.

The evolution of density matrix after a two-pulse sequence applied is described as

$$\begin{aligned}\boldsymbol{\rho}(t) = {} & \exp\left(-\frac{i}{\hbar}\boldsymbol{H_0}(t - \tau_1 - \tau - \tau_2)\right)\exp\left(-\frac{i}{\hbar}\boldsymbol{H_p}\tau_2\right)\\ & \times \exp\left(-\frac{i}{\hbar}\boldsymbol{H_0}\tau\right)\exp\left(-\frac{i}{\hbar}\boldsymbol{H_p}\tau_1\right)\times\boldsymbol{\rho_0}\exp\left(\frac{i}{\hbar}\boldsymbol{H_p}\tau_1\right)\\ & \times \exp\left(\frac{i}{\hbar}\boldsymbol{H_0}\tau\right)\exp\left(\frac{i}{\hbar}\boldsymbol{H_p}\tau_2\right)\\ & \times \exp\left(\frac{i}{\hbar}\boldsymbol{H_0}(t - \tau_1 - \tau - \tau_2)\right),\end{aligned} \quad (5)$$

where τ_1 and τ_2 are lengths of the two pulses, τ is the delay between two pulses, $t > \tau_1 + \tau + \tau_2$.

The ESE signal intensity was calculated using the equation:

$$f(B_0, t) = Tr\{\boldsymbol{\rho}(t)S_y\}. \quad (6)$$

3. Experiment

Fullerene C_{70} (Aldrich, 99% purity) was dissolved in decaline (1:1 mixture of *cis*- and *trans*-decalin, Sigma–Aldrich), at a concentration of about 3×10^{-4} M. Solution was put in a quartz tube of a 4.6 mm outer diameter. Three freeze-pump-thaw cycles were executed to remove air, and then tubes were sealed under vacuum. The samples were frozen, and the solution represented itself a transparent glass.

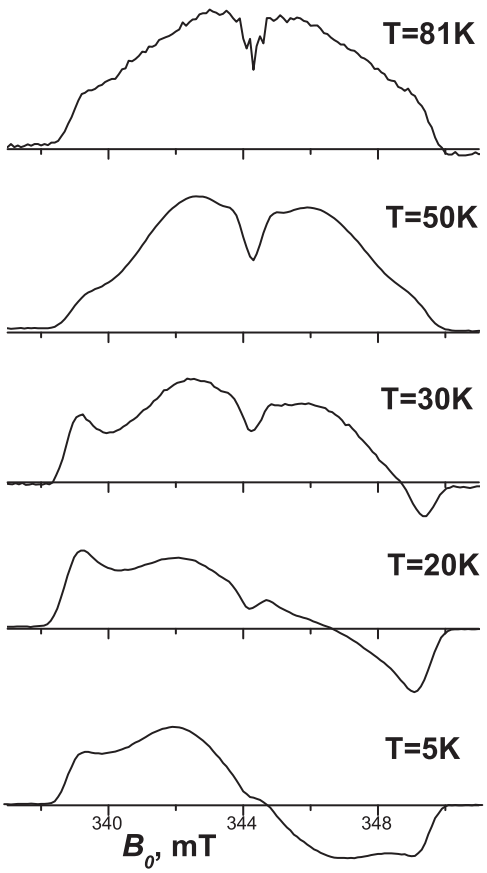

Fig. 1. ED EPR spectra obtained by 16 ns–120 ns–32 ns–*echo* pulse sequence at different temperatures. For convenience, spectra are artificially normalized to nearly the same amplitude.

EPR and ESE experiments were carried out on an X-band ELEXSYS ESP-580E EPR spectrometer equipped with a dielectric cavity (Bruker ER 4118 X-MD-5) inside an Oxford Instruments CF 935 cryostat. The mw frequency was 9.651 GHz. In conventional EPR studies, the cavity was critically coupled, while in ESE experiments it was overcoupled to obtain a dead time after pulses equal to ~100 ns. To obtain an echo signal, a two-pulse mw pulse sequence τ_1–τ–τ_2–*echo* was used. The echo signal in the time domain was integrated on a built-in spectrometer integrator.

For the sample photoexcitation we used continuous irradiation from a Xe lamp, with a filter transmitting in the range between 350 nm and 700 nm. The estimated light power reaching the sample was about 10 mW. Temperature was controlled by a cold nitrogen gas flow and measured with a copper-constantan thermocouple attached to the sample.

Simulations were performed using a MATLAB 7.0 program package.

4. Results and discussion

4.1. Experimental ED EPR spectra

Two-pulse echo signal taken at the scanning magnetic field (ED EPR spectrum) for $^3C_{70}$ in glassy decaline is shown in Fig. 1, for temperatures in the range of 5–81 K. Here, the pulse lengths are 16 ns (τ_1) and 32 ns (τ_2), for a $\pi/2$-pulse and π-pulse, respectively (with a delay τ of 120 ns between two pulses). The spectra are normalized

to the same maximal intensity. One can see in Fig. 1 that ED EPR lineshape below 30 K consists of absorptive and emissive parts. The emissive part increases with temperature decrease.

The spectrum at 5 K is very similar to ED EPR spectra obtained earlier for a spin-polarized state of $^3C_{70}$ generated by laser pulse [8]. For 5 K, spin-lattice relaxation time T_1 is much longer than the triplet lifetime, so the thermodynamic equilibrium cannot be achieved at this temperature. With temperature increase T_1 becomes smaller, this explains why the emissive part in ED EPR spectrum decreases (see Fig. 1). At 50 K the ED EPR spectrum consists only of absorptive part; so at this temperature thermal equilibrium takes place. Between 5 K and 50 K ED EPR spectra may be ascribed to the states possessing populations that are intermediate between the full spin-polarization and thermal equilibrium situations. With temperature increasing above 50 K EPR lineshape varies only weakly (see Fig. 1). Note however echo signal is decreasing remarkably above 50 K (data not given).

In the center of spectra in Fig. 1 a narrow hole appears. This feature in echo-detected EPR spectra, to our knowledge, has not been so far described in the literature. The hole width, estimated at its half-height, is around 0.6 mT. This value corresponds roughly to the microwave amplitude, B_1, of the pulses.

To investigate dependence of the hole on B_1, we also applied selective pulses, with $\tau_1 = 100$ ns and $\tau_2 = 200$ ns, for $\pi/2$-pulse and π-pulse, respectively (so $B_1 = 0.1$ mT). The obtained ED EPR spectrum is shown in Fig. 2 (solid line). Now the hole becomes much narrower, with the width approximately equal to 0.2 mT. So, the hole width decreases with B_1 decrease.

Note that in CW EPR the B_1 value is normally essentially smaller than that in ESE, which may explain why in CW EPR we did not observe such a central hole at temperatures of our experiment (data not given).

In Fig. 3 ED EPR spectra are given for $^3C_{70}$ in decaline at 70 K, obtained with $\tau_1 = 16$ ns and $\tau_2 = 32$ ns, and with varying B_1 amplitude. The latter was chosen so that turning angle of the first pulse, $\chi_1 = \gamma B_1 \tau_1$, was $\pi/2$, 0.7π, or π. One can see that with the angle increasing the broad line in the ED EPR spectrum is diminishing. This effect has a natural explanation because echo intensity in such experiment is expected to be proportional to $\sin^3(\chi_1)$ [13]. Meanwhile, the hole in the center of the spectrum does not disappear. Moreover, it becomes to be a dominating peak in the spectrum.

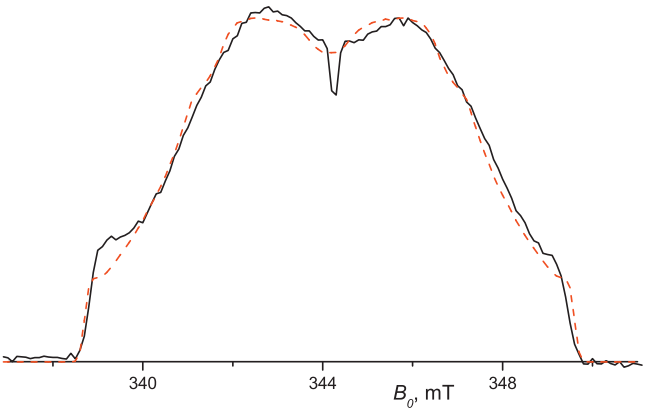

Fig. 2. ED EPR spectrum obtained by 100 ns–300 ns–200 ns–*echo* pulse sequence at 50 K (solid line). The dashed line represent simulation using a two-level system approximation, with the parameters $D = 5.45$ mT and E distributed uniformly in the range of 0.2–1.5 mT.

4.2. Simulation: two-level approach

In numerical simulations of EPR spectra we supposed Boltzmann distribution of spin populations between three spin sublevels, T_+, T_0, and T_-. ZFS parameter D was chosen to be equal to 5.45 mT, while E was randomly distributed within the range of 6–42 MHz. The time values of Eq. (5) were assumed the same as in experiment: $\tau_1 = 16$ ns, $\tau = 120$ ns, $\tau_2 = 32$ ns. In a simple two-level approach, EPR lineshape is obtained by averaging over angles θ and φ of the Gaussian individual line function $g(B)$:

$$G(B_0) = \frac{1}{4\pi} \iint \sin\theta \, d\theta \, d\varphi \left[g\left(B_0 - \frac{\hbar\omega_{0+}(\theta,\varphi)}{g\beta} \right) + g\left(B_0 - \frac{\hbar\omega_{0-}(\theta,\varphi)}{g\beta} \right) \right]. \quad (7)$$

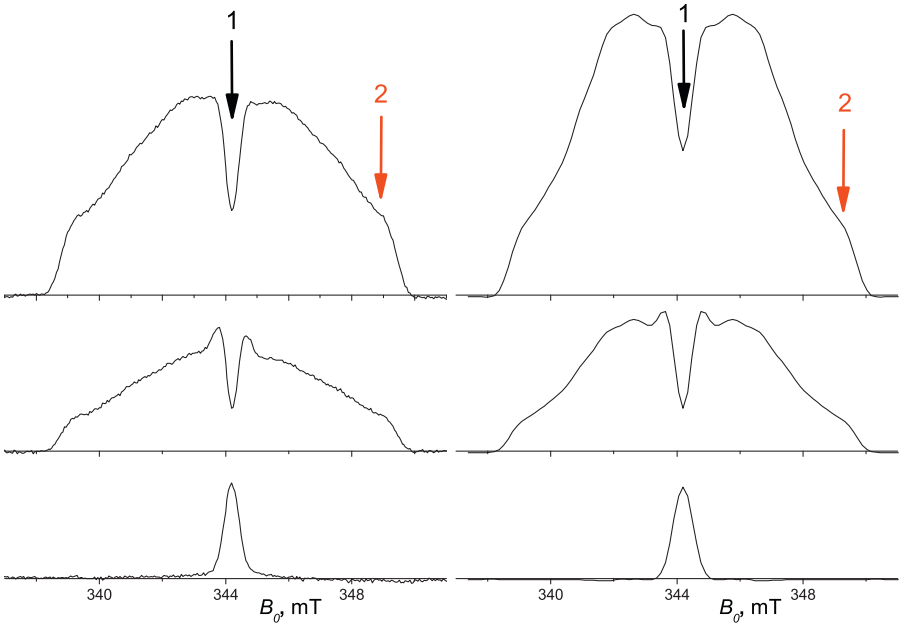

Fig. 3. ED EPR spectra obtained by 16 ns–120 ns–32 ns–*echo* pulse sequence with different mw pulse amplitudes. The turning angle of the first pulse (χ_1) corresponds to $\pi/2$ (a), 0.7π (b), and π (c). The curves d, e, and f are their simulation using the density matrix formalism (Eq. (8)), with the same D and E values as in Fig. 2. Simulated spectra are artificially normalized to provide approximately the same scale for curves b and e.

The $g(B)$ peak-to-peak linewidth, H_d, was taken as 0.1 mT.

The simulated ED EPR spectrum is presented in Fig. 2 as dash line. The simulation reproduces the experimental ED EPR spectrum everywhere, except for the center. So, we conclude that simple two-level approach is not applicable for the central region.

We supposed that this feature arises because in the center of the ED EPR spectrum the resonance energies for two allowed $T_+ \leftrightarrow T_0$ and $T_0 \leftrightarrow T_-$ transitions are equal (i.e., $\hbar\omega_{0+} = \hbar\omega_{0-}$, see Eq. (2)), so that mw pulses simultaneously excite both transitions. This suggestion is additionally supported by the experimental fact that width of the central hole was found to nearly match the microwave pulse amplitude B_1 (see above). Indeed, the equality of the two transition energies must be attained with accuracy determined by B_1, its decreasing diminishes the fraction of triplets for which two transitions are simultaneously excited.

4.3. Simulation: density matrix evolution

Numerical simulation of $^3C_{70}$ ED EPR spectra was performed by calculating evolution of the triplet density matrix (see Eq. (6)), assuming initial Boltzmann distribution of the T_+, T_0, and T_- populations, and with the same D and E values as in the previous case. ESE signal was integrated in the time domain, like as it was done in the experiment (see above), and over the θ and φ angles. For any given orientation, the offset frequency $\gamma B = \gamma B_0 - \omega$ (see Eq. (3)) was assumed to be distributed by a Gaussian law, with the width H_d of 0.1 mT – cf. Eq. (7). So, instead of Eq. (7), we have

$$F(B_0) \propto \iint \iint f(B,t) g(B_0 - B) \sin\theta \, d\theta \, d\varphi \, dB \, dt. \quad (8)$$

The parameter ω_1 (see Eq. (4)) was varied to match the different pulse amplitude used in the experiment.

The simulated spectra are shown in Fig. 3(d–f). One can see that under the used approach the features in the center of ED EPR spectra are reproduced nicely. For $\chi_1 = 0.7\pi$ (Fig. 3b and e), two peaks are arising at both sides of the central spectral hole. When $\chi_1 = \pi$ (Fig. 3c and f), the central hole is replaced by the central peak whereas the broad part of the spectrum disappears. Good agreement between the experimental and the simulated spectra confirms that the origin of the central features in the EPR spectra is simultaneous excitation of $T_0 \leftrightarrow T_+$ and $T_0 \leftrightarrow T_-$ spin transitions of $^3C_{70}$ by mw pulses. The high amplitude of these features is related to small anisotropy of g-tensor of $^3C_{70}$. For the case of negligible anisotropy of g-tensor, the degeneracy of $T_0 \leftrightarrow T_+$ and $T_0 \leftrightarrow T_-$ spin transitions for $^3C_{70}$ with different molecular orientations occurs at the same B_0 value, namely, at the center of $^3C_{70}$ ED EPR spectrum. While the influence of anisotropy of g-tensor of $^3C_{70}$ is small at X-band, it cannot be neglected at high-field, for example, at W-band [7,8]. In such conditions the spectral region of degeneracy of $T_0 \leftrightarrow T_+$ and $T_0 \leftrightarrow T_-$ spin transitions is extended, and the total amplitude of the corresponding features in ED EPR spectrum would be suppressed.

In Fig. 4 the simulation of the $^3C_{70}$ ESE signal intensity dependence on the turning angle χ_1 (χ_1–τ–2χ_1–echo pulse sequence) is presented, in comparison with the experimental data, for two different positions in the EPR spectrum. The simulation for position 2 is in agreement with experimental ESE intensity dependence and shows the typical behavior of a two-level spin system: ESE signal attains maximum for a $\pi/2$–τ–π–mw pulse pattern, disappears after π–τ–2π–pulse train, and inverts with further increase of the mw pulse power. Note that this simulated dependence is nicely approximated by a $\sin^3(\chi_1)$ function, which is predicted by a simple formula describing the echo formation in two-level system [13] (data not given).

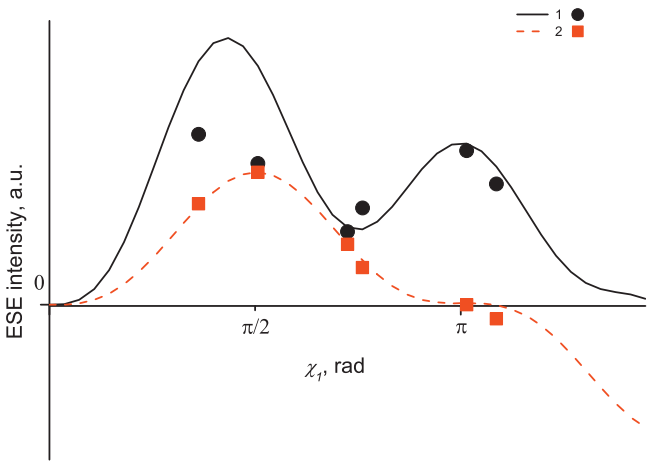

Fig. 4. ESE signal intensity dependence on the turning angle of the first pulse, χ_1, in a χ_1–τ–2χ_1–*echo* sequence. Solid line – position 1 in ED EPR spectrum (see Fig. 3), dashed line – position 2. The experimental ED EPR spectral intensities are given by circles (position 1) and squares (position 2) (cf. Fig. 3a, b, c).

Such a simple analytical formula cannot be obtained for the complicated case of ESE formation in three level system with excitation of both allowed transitions. The calculation for this case based of Eqs. (3)–(6) with zero ZFS parameters D and E (i.e., with $T_0 \leftrightarrow T_+$ and $T_0 \leftrightarrow T_-$ transitions strictly degenerate) predicts the $\sin^3(\chi_1)$ dependence of ESE intensity, similar to the two-level system (data not shown). However, it does not agree with the experimental dependence of ESE at the center of the ED EPR spectrum (position 1 in Fig. 4) even qualitatively. On the other hand, the simulation of the ESE signal intensity dependence for this position based complete spin-Hamiltonian of $^3C_{70}$ reasonably reproduces the observed behavior (circles in Fig. 4). This means that for description of this phenomenon not only the simultaneous excitation of both spin transitions of the triplet by mw pulses, but also the interplay of ZFS interaction and B_1 during the echo-forming mw pulses should be taken into account. This is further confirmed by our observation that the pulse angle dependence of $^3C_{70}$ ESE intensity for the position 1 changes with variation of E distribution (data not given).

Some discrepancy between the experimental and simulated ESE dependence of the central hole seen in Fig. 4 (especially for $\chi_1 = \pi/2$) may occur because mw pulses are not perfectly rectangular, so the Hamiltonian in Eq. (4) describe the experimental situation only approximately. Additionally, the real distribution of E may differ from the rectangular one.

Note that appearance of a hole in EPR spectrum is also observed in continuous wave saturation transfer EPR experiments on nitroxide spin labels [14,15]. In these experiments EPR spectra are recorded with a $\pi/2$ phase shift of the magnetic field modulation (out-of-phase EPR detection), under conditions of mw power saturation of EPR transitions. Slow molecular tumbling partly removes saturation, which results in appearance of "holes" in some regions of the spectrum. Their depths, like in our case, also increase with mw power increase. However this effect cannot be related with the phenomenon observed here, because it is not connected with the degeneracy of electron spin transitions.

5. Conclusion

ED EPR spectra of $^3C_{70}$ generated by continuous light illumination were detected at different temperatures. Above 50 K ED EPR spectra correspond to equilibrium Boltzmann population distribution within triplet sublevels. At lower temperatures the non-equilibrium polarizations of triplet sublevels arose due to the dominance of triplet decay process over spin-lattice relaxation.

We found that ED EPR spectra of $^3C_{70}$ in glassy matrices at temperatures higher than 50 K may be simulated with ZFS parameters: D = 150 MHz, and E distributed uniformly in the range of 6–42 MHz. Since C_{70} has D_{5h} symmetry, which implies the axial ZFS tensor, the non-zero E value indicates the distortion of $^3C_{70}$ due to Jahn–Teller effect. The most probable origin of E distribution is dependence of the Janh–Teller effect in $^3C_{70}$ on the local surrounding of fullerene molecule in glassy matrices (a so-called E-strain).

The hole observed in the center of $^3C_{70}$ ED EPR spectra originates from the simultaneous excitation by mw pulses of the two allowed spin transitions $T_0 \leftrightarrow T_+$ and $T_0 \leftrightarrow T_-$ of the triplet. It is characterized by an anomalous pulse angle dependence of the ESE intensity. The widely used two-level system approximation does not describe this spectral feature, while strict simulations based on the density matrix evolution of the S = 1 three-level system reproduces this result nicely.

This effect may be probably used to select the $^3C_{70}$ ESE signal in complicated systems.

Note that in experiments in which $^3C_{70}$ is produced by a laser pulse [4,5,8,9] the ESE signal in thermal equilibrium cannot been observed, because it requires long time delays after the laser flash, and laser repetition rate normally is too low to accumulate the signal. So the central hole like that found here cannot be detected. In CW EPR the microwave pulse amplitude is normally small, as compared with that in ESE, so under continuous light irradiation such a central hole here also cannot be observed (at least at temperatures of our experiment).

6. Acknowlegement

This work was supported by program of Presidium of Russian Academy of Sciences, project # 27.55.

References

[1] R. Signorini, in: J. Shinar, Z.L. Vardeny, Z.H. Kafafi (Eds.), Optical and Electronic Properties of Fullerenes and Fullerene-Based Materials, Marcel Dekker, NY, 2001, p. 295.
[2] A. Hirsch, M. Brettreich, Fullerenes: Chemistry and Reactions, Wiley-VCH, Weinheim, 2005, pp. 33–38.
[3] M.N. Uvarov, L.V. Kulik, M.A. Bizin, V.N. Ivanova, R.B. Zaripov, S.A. Dzuba, J. Phys. Chem. A 112 (2008) 2519–2525.
[4] M.N. Uvarov, L.V. Kulik, S.A. Dzuba, J. Chem. Phys. 131 (2009) 144501.
[5] M.R. Wasilewski, M.P. O'Neil, K.R. Lykke, M.J. Pellin, D.M. Gruen, J. Am. Chem. Soc. 113 (1991) 2774–2776.
[6] K.D. Ausman, R.B. Weisman, Res. Chem. Intermed. 23 (1997) 431–451.
[7] X.L.R. Dauw, J. Visser, E.J.J. Groenen, J. Phys. Chem. A 106 (2002) 3754–3758.
[8] X.L.R. Dauw, O.G. Poluektov, J.B.M. Warntjes, M.V. Bronsveld, E.J.J. Groenen, J. Chem. Phys. A 102 (1998) 3078–3082.
[9] G. Agostini, C. Corvaja, L. Psimeni, Chem. Phys. 202 (1996) 349–356.
[10] M. Terazima, K. Sakurada, N. Hirota, H. Shinohara, Y. Saito, J. Phys. Chem. 97 (1993) 5447–5450.
[11] H. Levanon, V. Meiklyar, S. Michaeli, D. Gamliel, J. Am. Chem. Soc. 115 (1993) 8722–8727.
[12] E. Wasserman, L.C. Snyder, W.A. Yager, J. Chem. Phys. 41 (1964) 1763–1772.
[13] A. Schweiger, G. Jeschke, Principles of Pulse Electron Paramagnetic Resonance, Oxford University Press, NY, 2001.
[14] J.S. Hyde, L. Dalton, Chem. Phys. Lett. 16 (1972) 568–572.
[15] D.D. Thomas, J.S. Hyde, L. Dalton, J. Chem. Phys. 65 (1976) 3006–3024.